Final submitted manuscript: published in Construction and Building Materials 304 (2021) 124588

Improved indirect measurement of the dynamic stiffness of a rail fastener and its dependence on load and frequency

Qi Li[1], Baorui Dai[1], Zhihui Zhu[2, 3*], David J. Thompson[4]

[1] Department of Bridge Engineering, Tongji University, Shanghai 200092, China
[2] School of Civil Engineering, Central South University, Changsha 410005, China
[3] National Engineering Laboratory for High-Speed Railway Construction, Changsha 410005, China
[4] Institute of Sound and Vibration Research, University of Southampton, Southampton SO17 1BJ, United Kingdom

Abstract

The dynamic stiffness of rail fasteners has a significant effect on the noise radiated by the rails as well as the vibration transmitted to the underlying structures, such as bridges, tunnels or track at grade. This study investigates the load- and frequency-dependence of a WJ-2A fastener which is commonly used in urban rail transit systems in China. This is a two-stage fastener with a rail pad and a baseplate pad separated by a steel plate. Results are obtained using the indirect measurement method in the frequency range 30 to 1000 Hz. The dynamic stiffness of the individual components is investigated as well as that of the whole fastener system and the combined stiffness of the components is verified by comparison with the whole fastener system. A numerical model of the test rig is used to provide understanding of various artefacts that are observed in the measurements and corrections are proposed to minimise their effects on the measured results. These allow for the differences between the response at the measurement positions and at the ideal positions at the interfaces between the fastener system and the rig. The stiffness magnitude of the rail pad, baseplate pad, and whole fastener system increases strongly with increasing static preload and increases weakly with increasing frequency; it is important to take these effects into account in prediction models for noise and vibration. The damping loss factors are not strongly dependent on preload or frequency. To describe the frequency-dependence, a fractional derivative Kelvin-Voigt (FDKV) model is introduced and is fitted to the dynamic stiffness with the help of a genetic algorithm method.

The dynamic stiffness of the whole fastener system is influenced by both the rail pad and the lower baseplate pad. It is important to take account of both of them, as well as the internal resonance of the baseplate assembly which appears at around 1 kHz.

Keywords

rail fastener; viscoelasticity; experimental study; load-dependent; frequency-dependent; dynamic stiffness

1 Introduction

As vital components of the track structure, the rail fasteners connect the rails to the sleepers or track slab, or directly to bridges, and play the role of transferring loads to the supporting structure while also providing appropriate resilience. To reduce the vibration and noise transmission, rubber components known as rail pads are introduced within the fastener systems. Due to the viscoelasticity and nonlinearity of the rubber materials [1], and sometimes their geometrical nonlinearity (e.g. ribbed or studded rail pads) [2], the dynamic properties of the rail pads contain noticeable dependence on load and frequency.

Numerous studies have been carried out to investigate the influence of the dynamic properties of the rail pads on the vibration and noise of railway track and the coupled vehicle-track system. Sol-Sanchez et al. [3] reviewed the problems and test method associated with elastic elements (e.g. rail pads, under-sleeper pads, and under-ballast mats) in the railway track. Knothe and Grassie [4] reviewed models of railway track and vehicle/track interaction at frequencies above 20 Hz and pointed out the importance of the rail pad for the dynamic behaviour. Carrascal et al. [5] compared the stiffness, fatigue aging and other properties of a metal cushion pad with plastic pads, showing the dynamic stiffness of various pads was dependent on the excitation frequency in the direct measurement. Vincent et al. [6] conducted a parametric study on the effect of rail pad stiffness on the noise radiated by railway track and showed that stiffening the rail pad reduced the noise radiation from the rail whereas it increased

that from the sleeper. Oregui et al. [7] analysed the effect of the dynamic behaviour of the rail pad on the vibration response of tracks with monoblock concrete sleepers. The results showed that, to reproduce the measured characteristics of the tracks in a specific frequency range, the frequency-dependent stiffness of the rail pad should be considered. Zhu et al. [8] developed an improved vehicle-track dynamic model by introducing the frequency- and amplitude-dependent properties of rail pads. The dynamic responses obtained from their model were shown to be related to the dynamic properties of the rail pads, in both frequency and time domain. By studying models of high-speed vehicles and track, Wei et al. [9, 10] found that the dynamic properties of the rail pads have a significant influence on the vibration of the rails, car bodies, bogies, etc. in the medium- and high-frequency ranges.

Considering the temperature-dependent properties of the rail pads, Squicciarini et al. [11] conducted a field test to measure the noise from passing trains at various temperatures from 0 to 35°C. The measured results showed that the noise increased with the increase of temperature. This was consistent with the measured rail pad stiffness and track decay rates which reduce at higher temperatures. In terms of the load dependence effects of rail pads, Thompson et al. [12] assessed, through simulations, the noise radiated from a track containing typical soft pads. Neglecting the load dependence of the rail pads was found to overpredict the track noise, which indicated that the increase in noise with softer pads was less severe than previously suggested. It is clear that it is important to take proper account of the dynamic behaviour of the rail pads in the analysis of vibration and noise to achieve suitable calculation accuracy [11, 13].

Over the last 30 years, a variety of experiments have been performed to determine the dynamic properties of the rail pads. A set of standards related to laboratory measurement methods has been produced to guide the testing of resilient elements [14-16]. The test methods can be divided into two main types, known as the direct method and the indirect method. In the direct method the transmitted force is measured directly, while in the indirect method the force

is derived from the dynamic response of a suspended mass [17]. Several publications have addressed the application of the direct method in the measurement of the frequency-dependent properties of resilient elements [5, 18, 19]. However, the direct method is limited to relatively low frequencies and a single measurement direction [20]. Conversely, the indirect method is more suitable for higher frequencies and can be used for multiple directions. Thompson et al. [2, 20] and Fenander [21] used the indirect method to measure the dynamic properties of rail pads under different preloads. The test rig and the test element were modelled as a multi-body system with two degrees of freedom, excited by a dynamic exciter. In addition, an instrumented hammer can also be considered as an alternative method of excitation. Van't Zand [22] and De Man [23] developed a resonant apparatus called a rail pad tester and excited it with an impact hammer to assess the stiffness and damping of rail pads. Remennikov and Kaewunruen [17, 24] developed a methodology based on the impact hammer technique to determine the dynamic properties of rail pads, and demonstrated the effect of preload on these properties. Kaewunruen and Remennikov [25, 26] also developed a method to measure the dynamic properties of the track in the field using impact excitation for the evaluation of the track state. Due to the ability to control the temperature and preload simultaneously, universal testing machines are often used to measure the temperature dependence of whole rail pads or pad specimens. Wei et al. [27, 28] conducted an experimental study on the temperature-dependent properties of whole rail pads using a universal testing machine, and used the Williams-Landel-Ferry formula [29] relating temperature- and frequency-dependence to predict the frequency-dependent properties of the pads. Liu et al. [30] tested cylindrical specimens from a rail pad, with diameter 15 mm and height 10 mm, to extract the temperature-dependent Young's modulus; temperature sweep tests were performed with the help of a dynamic mechanical testing machine. The temperature-dependent stiffness of the rail pad was obtained and then considered in a vehicle-track-viaduct vertical coupled model. These various experimental studies have proposed effective methods

and designed practical test rigs, using both direct and indirect methods, which can be adopted to measure the dynamic properties of rail pads.

To take the dynamic properties of rail pads into account in the theoretical analysis of structural vibration or noise, suitable mathematical models for the stiffness and damping should be established. In general, temperature- and load-dependent properties can be based on simple curve-fitting whereas the frequency-dependent properties are described by more complex models, especially if the viscoelastic characteristics are to be introduced into time domain analysis. The traditional models combining springs and dashpots, the Kelvin-Voigt and Maxwell models, have been widely used in characterizing viscoelastic materials [31-33]. However, the ordinary Kelvin-Voigt and Maxwell models are limited in their ability to describe the frequency-dependence of the dynamic stiffness of rail pads [8, 32]. Although extending such models with additional springs and dashpot elements can achieve a better approximation of the frequency dependence, the complexity of the model fitting increases considerably.

An alternative method to express the frequency-dependence of the dynamic characteristics of rail pads is to use the constitutive relations that introduce fractional order derivatives. In general, fractional order derivatives can be considered as an interpolation between the elastic and viscous behaviour of rubber components [34]. Compared with the traditional models, fractional derivative models require fewer parameters to accurately characterize the complex behaviour of viscoelastic materials [35, 36]. Caputo is one of the pioneers who introduced fractional derivative operators to describe viscoelasticity and presented a proper mathematical definition [37]. Since then, the efficiency of the fractional derivative models in describing the behaviour of rubber pads has been extensively demonstrated [21, 27, 38, 39].

Generally, fastener systems used on slab tracks, bridges and in tunnels contain not only rubber materials but also a steel baseplate. Due to the influence of inherent resonances of the steel plate, the dynamic behaviour of the whole fastener is different from that of the rubber

materials alone.

This study aims to investigate experimentally the dynamic properties of a whole fastener assembly, as well as the individual fastener components. A test rig is designed for measuring the load- and frequency-dependent properties of the test elements under hydraulic preloads and dynamic excitation, based on the indirect method [20]. An enhancement of the experimental method is proposed on the basis of theoretical analysis and numerical simulation. The frequency-dependent stiffness values and damping loss factors of the whole fastener assembly and fastener components are obtained and then represented by linear functions in double logarithmic coordinates. A comparison is also presented of the results for the whole fastener assembly and the combination of the results for the components. The stiffness values and damping loss factors are then fitted by a fractional derivative Kelvin-Voigt (FDKV) model through parameter identification using a genetic algorithm method [40] in the frequency domain. It is expected that the dynamic properties of the whole fastener and the fastener components obtained in this experimental study will contribute to improving the calculation accuracy of models for the vibration and noise of track systems in both the frequency and time domain.

2 Experimental method

2.1 Experimental preparation

A full-size WJ-2A rail fastener, a type used widely in urban rail transit in China, was prepared for the dynamic performance test. As a shoulderless structure, the WJ-2A fastener system is composed of a rail pad, a steel plate and a second rubber pad beneath it, as shown in Figure 1a. The steel plate has a mass of 10.05 kg. The rail pad is a ribbed thick plate (see Fig. 1b) and the lower baseplate pad is flat thin plate (see Fig. 1c). They are made of viscoelastic materials, thermoplastic polyester elastomer (TPEE) and thermoplastic vulcanizate (TPV) respectively. The static stiffness of the rail pad as specified by the manufacturer is about 40 MN/m, obtained from the average relative compression of the pad subjected to a vertical load

of 10 kN and 50 kN. The dynamic stiffness of the pad should not be larger than 1.25 times the static stiffness, which is obtained by the manufacturer from a harmonic load between 10 kN and 50 kN and at a frequency of 4 Hz. The static and dynamic stiffness obtained by the above methods can be used to evaluate the manufacturing quality of rail pads. However, they are not suitable to be adopted in the noise prediction of the rail and bridge up to 1000 Hz because the pad stiffness is generally larger at these high frequencies and the corresponding small strain amplitudes [2]. The indirect measurement method is thus utilized in this study to obtain the frequency dependent dynamic stiffness of the fastener. Although new pads were tested in this study, deteriorated pads can be also tested by this method to evaluation of their performance after years of service.

In this test, the dynamic stiffness is measured of the whole fastener unit, the rail pad, and the baseplate pad (in combination with the steel plate). The behaviour is represented by a frequency-dependent complex dynamic stiffness $K(f) = K_r(f)(1 + \mathrm{i}\eta(f))$ where K_r is the real part of the complex stiffness, f is frequency, η is the loss factor and i is the imaginary unit. If the lower face of the sample is constrained and a displacement of amplitude $X(f)$ is applied to the upper face, the force transmitted to the blocked termination is given by $K_{12}(f)X(f)$ and the reaction force at the upper face is $K_{11}(f)X(f)$ where K_{11} is the drive point dynamic stiffness and K_{12} is the transfer stiffness. At low frequency they are identical. The measurement method is intended to obtain the transfer stiffness.

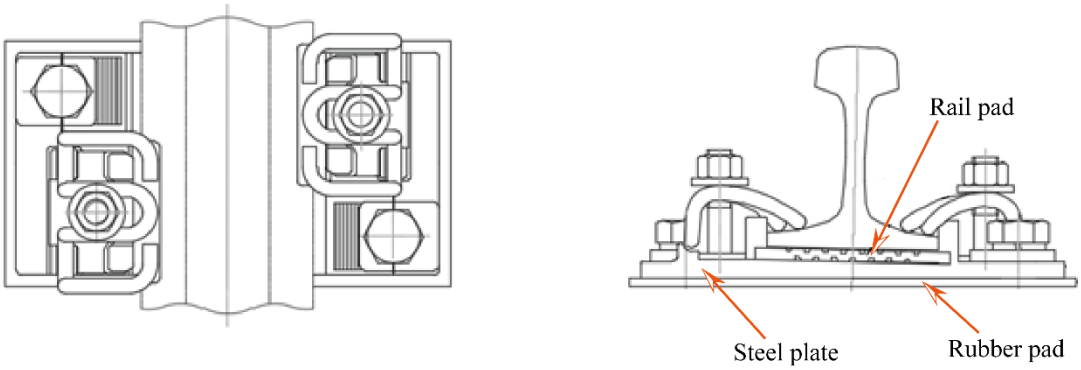

(a) components of the fastener

(b) rail pad

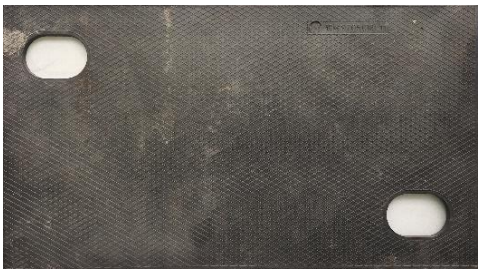

(c) baseplate pad

Figure 1. Structure of WJ-2A rail fastener and the associated pads

In the test rig (Figure 2), a large steel block of dimensions 35 cm × 74 cm × 104 cm (height × width × length) and mass 2128 kg is supported by resilient mounts on a strong floor. The test element is mounted on the top surface of this block and a short length of rail is attached above the test element, allowing rail clips to be installed as required. The top of the rail head was machined flat and a loading plate was attached to it. Above this, resilient mounts support a further steel loading plate, above which is the hydraulic loading system. This is used to introduce a static preload whereas dynamic excitation is introduced by an inertial exciter of mass 5 kg attached above the rail. A pair of accelerometers (numbered A1 and A2) are attached on either side of the rail head and used to measure its vertical vibration; using their average signal eliminates any effect of rotation. Another pair of accelerometers (A3 and A4) are fixed on the upper surface of the block on either side of the test element and their signals are averaged to obtain the vertical vibration of the block. Compared with the similar test rig used in [2, 20, 21], the main difference is the inclusion of a section of rail for the attachment of the rail clips and fasteners; this together with a loading plate forms the upper ‘mass’.

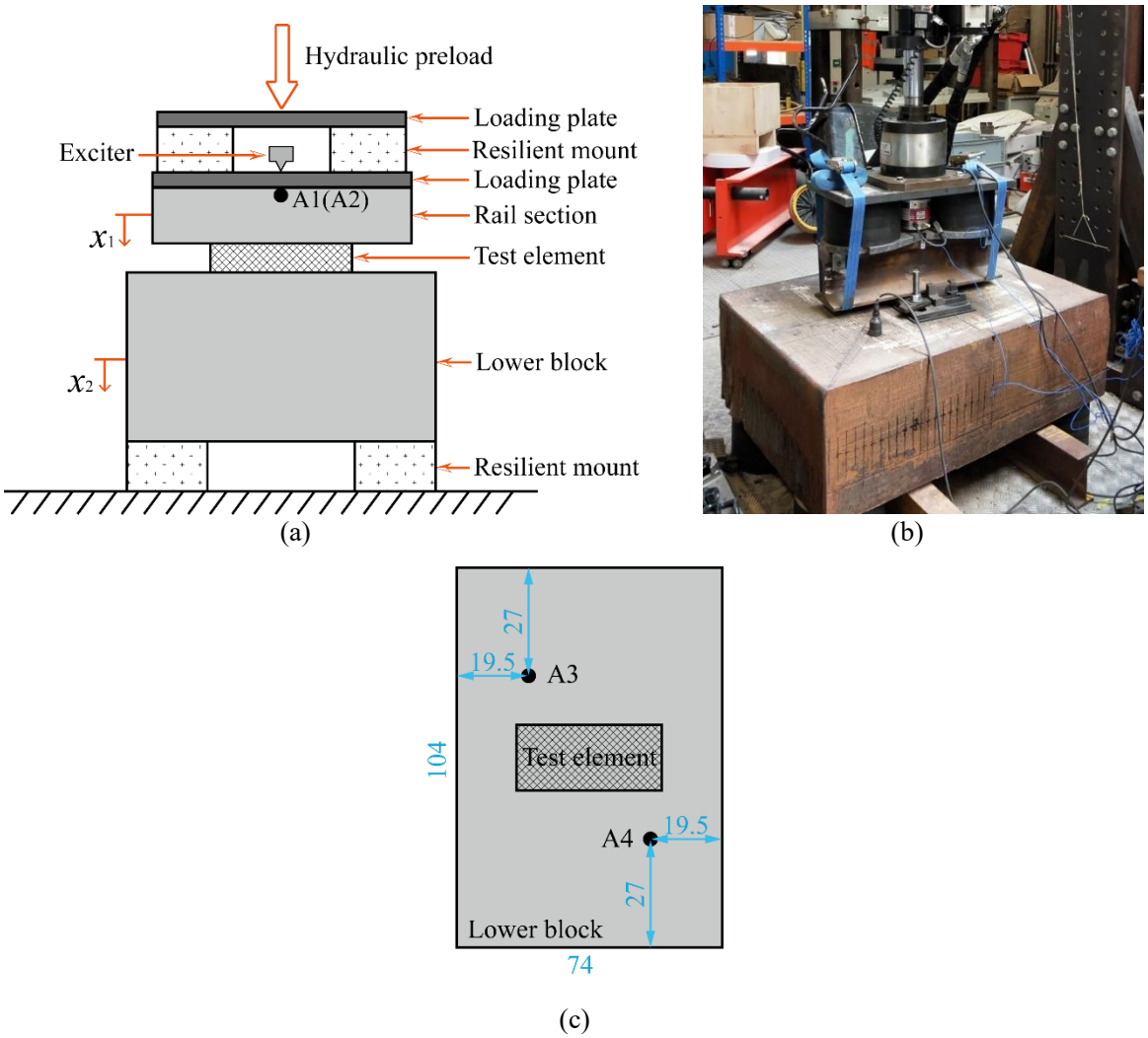

Figure 2. Test rig for measuring the dynamic properties of rail fasteners: (a) schematic diagram; (b) photograph; (c) measuring points position, top view (unit: cm)

Considering the typical wheel load, the maximum static load for a single fastener is about 40 kN. Additionally, the rail clips introduce a nominal preload of 20 kN on the rail pads. Therefore, preload values from 20 to 50 kN were used, with intervals of 5 kN, with additional results obtained for preloads up to 80 kN in some cases. The test is carried out using a pseudo-random force time-history and the results were then transformed into the frequency domain by using Fourier transforms. This allows all frequencies of interest to be measured simultaneously. The force signal was generated by the analyser and covered the frequency range up to 2500 Hz. During the test, the temperature in the laboratory was kept around 20 ℃ to avoid temperature variations.

2.2 Experimental principle

The experimental rig is designed to measure the dynamic properties of test elements, i.e. the dynamic stiffness and damping loss factor, under the combination of a static preload and dynamic excitation. If it is assumed that the rail section and the large lower block have no elastic deformations, and for harmonic motion at circular frequency ω, the dynamic equilibrium equation of the block can be written as follows:

$$K(x_1 - x_2) = K_2 x_2 - m_b \omega^2 x_2 \tag{1}$$

where K is the complex dynamic stiffness of the test element, K_2 is the total dynamic stiffness of the elastic supports beneath the lower block, m_b is the mass of the lower block, and x_1 and x_2 are respectively the vertical displacement amplitudes of the rail section and the lower block.

By rearranging this and substituting displacements with accelerations, the dynamic stiffness of the test element can be expressed as:

$$K = (K_2 - m_b \omega^2) \frac{x_2}{x_1 - x_2} = (K_2 - m_b \omega^2) \frac{a_2}{a_1 - a_2} \tag{2}$$

where a_1 and a_2 are respectively the vertical acceleration amplitudes of the rail section and the lower block. In the above equation, K can be determined from the measured accelerations of the rail and the block if m_b and K_2 (stiffness of the resilient mounts) are known. However, previous studies [2, 41, 42] often used formulae that ignore K_2 to represent K as:

$$K \approx -m_b \omega^2 \frac{a_2}{a_1 - a_2} \tag{3}$$

At high frequencies, the result obtained by Eq. (3) is in good agreement with that obtained by Eq. (2) because K_2 is significantly smaller than $m_b \omega^2$, while at low frequencies there is a large difference between them because K_2 and $m_b \omega^2$ have similar magnitudes around the natural frequency of the block sitting on the mounts. Thus, it is preferable to obtain the value of K_2. This has been achieved by means of a simple hammer test on the lower block

disconnected from the fastener and loading system. The block and its elastic supports can be simplified as a single-degree-of-freedom mass-spring system; then the stiffness of the mounts can be expressed as:

$$K_2 = m_b(2\pi f_0)^2(1 + \mathrm{i}\eta) \tag{4}$$

where f_0 is the fundamental resonance frequency of the mass-spring system and η is its damping loss factor.

After impacting the centre of the upper surface of the block with a hammer, when the fastener and upper part of the test rig had been removed, its acceleration was obtained through the accelerometers A3 and A4. The acceleration amplitude in the time domain showed an exponential decay, from which the loss factor η can be calculated by the logarithmic decrement method [43]. Its value is found to be 0.10.

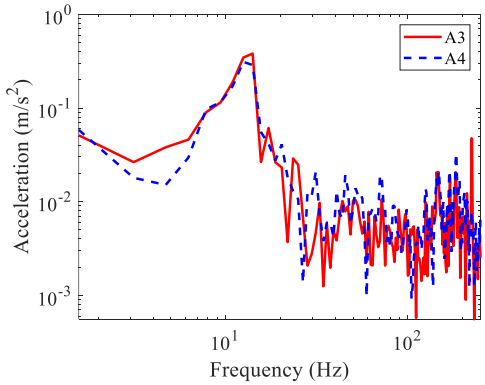

Figure 3. Spectra of the measured acceleration subjected to hammer impact for A3 and A4

The acceleration spectra of the lower block obtained from the two accelerometers are shown in Figure 3. From this the fundamental resonance frequency of the system is identified as about 14 Hz. It is worth noting that the stiffness of the resilient mounts below the lower block is slightly load-dependent. However, this property was shown to have only a small effect on the dynamic test results of the fasteners and was therefore neglected in the following analysis.

3 Numerical simulation of the test rig

3.1 Finite element model

Before presenting results from the measurements, in order to verify the correctness of the test results using the aforementioned test rig and data analysis method, a finite element model was established using solid elements (Solid95) in the commercial software ANSYS to represent the test rig. The elastic modulus of the rubber and steel material were assigned as 4.15 MPa and 2.1×10^5 MPa respectively, and their damping loss factors were set to be 0.06 and 0.02 respectively. The dimensions of all the components in the finite element model are consistent with the actual dimensions in the test. The density of the steel material and the resilient mount were set as 7900 kg/m^3 and 1000 kg/m^3 respectively. The mass of the rubber pads was ignored in the modelling so the stiffness of the rubber pads is assumed to be frequency-independent. Figure 4(a) shows the finite element model corresponding to the experiment for the whole WJ-2A fastener. This simulation was also carried out for the separate fastener components. From top to bottom, the finite element model consists of loading plate, rail section, test element, lower block and resilient mount, which are respectively connected by common nodes at the interfaces. The additional mass of the test equipment (excluding the exciter) above the steel plate was considered by introducing point mass elements. The elastic supports below the lower block were modelled as four supporting columns. For the supporting columns, all degrees of freedom of the bottom nodes and the horizontal degrees of freedom of the residual nodes were constrained. The degrees of freedom of other nodes in the finite element model were kept unconstrained. To make the finite element model consistent with the test rig, the stiffness of the supporting columns was chosen to give the correct resonance frequency of the lower block on the mounts.

Direct harmonic analysis was performed with a concentrated force applied vertically at the centre node at the top of the rail section (corresponding to the location of the exciter). The responses of the finite element nodes corresponding to the measurement points (A1-A4) were obtained at frequencies from 5 Hz to 2000 Hz, with an increment of 5 Hz.

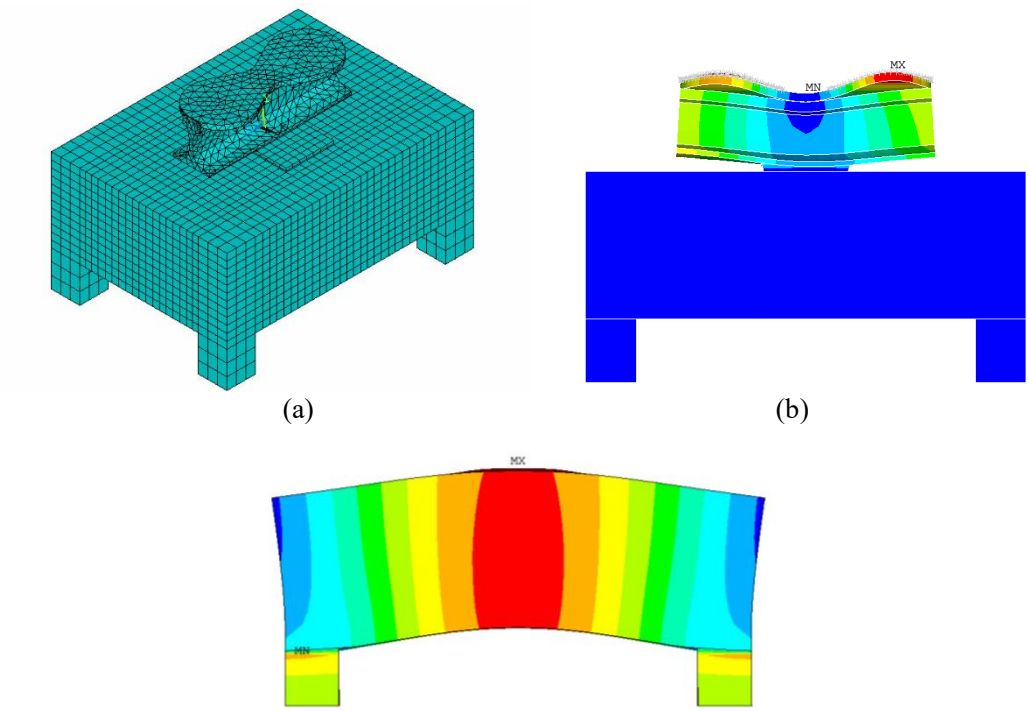

Figure 4. Finite element model and typical dynamic deformations of the test rig at different excitation frequencies: (a) finite element model; (b) deformation of the rail, 910 Hz; (c) deformation of the lower block, 1470 Hz

Figures 4(b) and 4(c) give typical dynamic deformations of the rail section and lower block. From this, it is clear that both the rail section and the lower block show local deformations in the high frequency region and therefore they cannot be simply regarded as rigid bodies. The accelerometers used in the test capture the vibration of the measurement points, but do not necessarily reflect the displacements input to the test elements or the transmitted forces. Therefore, it is useful to derive the relationship between the vibration responses of the measurement points and the responses of the test elements, in order to lay the foundation for determining the stiffness of the fastener system more accurately. The finite element model is used to simulate the dynamic stiffness measurement of the fastener system and to derive a revised method considering the local vibration of the rail and lower block in the high frequency range.

3.2 Stiffness estimation based on simulated acceleration of the lower block

An idealised measurement method would be based on the vibration of the upper and lower

surfaces of the fastener system. This can be simulated with the FE model but cannot be measured in practice. Taking into account the local vibration of the bodies, the equilibrium equation of the lower block can be established as:

$$K(x_{f1} - x_{f2}) = a_b/A_b \tag{5}$$

where K is the dynamic stiffness of the fastener; x_{f1} and x_{f2} are the overall (averaged) displacement amplitudes of the upper surface and lower surface of the fastener system, respectively; a_b is the average acceleration of the two nodes in the finite element model with the same positions as the measurement points on the surface of the block, and A_b is the average transfer accelerance from the lower surface of the fastener system to the positions A3 and A4.

To determine x_{f1} and x_{f2} weighting factors are introduced according to the surface area associated with each node in the finite element mesh, and then a weighted average of the displacements of all nodes in the corresponding interfaces is taken to represent their overall displacements. The dynamic stiffness of the fastener at circular frequency ω can be expressed as:

$$K = \frac{a_b\omega^2}{A_b(a_{f2} - a_{f1})} \tag{6}$$

where a_{f1} and a_{f2} are the averaged vertical acceleration amplitudes of the upper and lower surfaces of the fastener system. This idealised method should represent the dynamic stiffness correctly but cannot be used for practical measurements. Nevertheless, it will be used as the basis for correction factors derived below.

3.3 Simulation of test results

To simulate the test process described in Section 2, the responses of the four nodes in the finite element model corresponding to positions A1-A4 are used to represent the measured responses. Figure 5 shows the dynamic stiffness (magnitude) curves obtained by simulating the test method in Section 2, with and without including the support stiffness K_2 (i.e. using Eq. (2)

or (3)), and the idealised method proposed in the previous section based on the vibration response at the interfaces of the resilient elements and the test rig. Simulated results are shown for a 'measurement' of the rail pad, the baseplate pad (including the steel plate) and the whole fastener assembly.

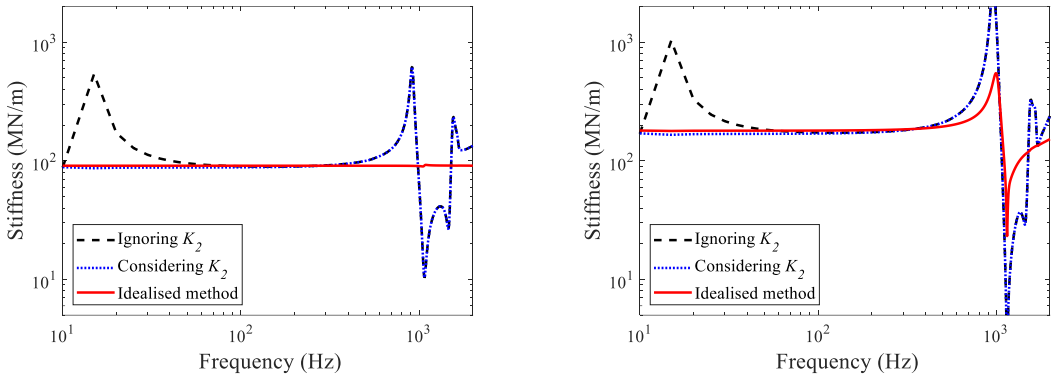

(a) rail pad (b) baseplate pad

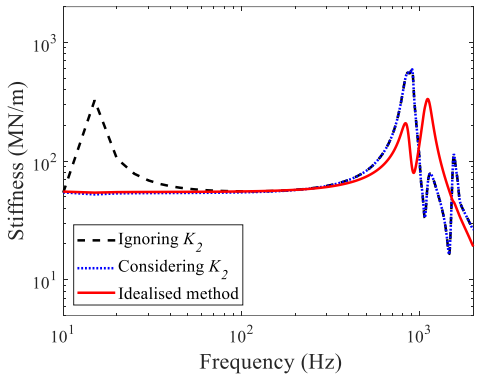

(c) whole fastener

Figure 5. Simulated stiffness magnitude plotted against frequency derived from three methods

In each case the curve derived from Eq. (3), ignoring the stiffness of the resilient mounts K_2, has a significant peak at low frequency which is eliminated by including K_2 (i.e. using Eq. (2)). However, at high frequencies the dynamic stiffness obtained from both of these simple methods is quite different from the idealised method. For the rail pad (Figure 5(a)), the dynamic stiffness obtained using the idealised method is basically a constant value which is equal to the stiffness introduced into the finite element model of the rail pad (which has no mass), indicating that the peaks and dips in the stiffness curves obtained from the simple methods (seen in Section

4 below) are the result of the test rig dynamics. For the baseplate pad and whole fastener (Figure 5(b) and 5(c)), the results derived from the idealised method gradually increase and then fluctuate above 600 Hz and 400 Hz respectively, which is due to the internal resonances of the test elements.

3.4 Modification of test results

In view of these discrepancies between the different estimates, the test results should be obtained from a modified version of Eq. (2) by establishing the relationships between the response at the two sides of the resilient element and the responses at the corresponding accelerometer positions. For this, two modification factors are derived using the FE model. The first, H_1, represents the transmissibility from the response of A1/A2 (the two accelerometers on the side of the rail head) to the vibration of the contact surface between the bottom of the rail and the fastener. This is obtained from the FE model and defined as

$$H_1 = a_{f1}/a_u \tag{7}$$

where a_u is the averaged vertical acceleration of the two nodes in the finite element model with the same positions as the measurement points on the side of the rail head.

The second modification factor H_2 represents the transmissibility from the average response of A3/A4 (the two accelerometers arranged on the lower block) and the vibration of the contact surface between the lower block and the fastener, which is similarly defined as

$$H_2 = a_{f2}/a_b \tag{8}$$

Both factors are determined for loading at the rail head but they are independent of the resilient element under test. By substituting the two modification factors into Eq. (6), the modified dynamic stiffness estimate K_m of the fastener can be obtained as:

$$K_m = \frac{a_b\omega^2}{A_b(H_2a_b - H_1a_u)} \tag{9}$$

where, by comparison with Eq. (2) the mass m_b has also been replaced by the inverse of A_b, which is the average transfer accelerance from the lower surface of the fastener system to the

positions A3 and A4 in the frequency domain.

The modification factors including the transfer accelerance A_b (shown normalised by multiplying by the block mass m_b) obtained from the finite element model are shown in Figure 6(a). It can be seen that H_1, H_2 and $A_b m_b$ depend on frequency. In the low frequency range, the two modification factors H_1 and H_2 are approximately equal to 1, whereas in the high frequency range, they fluctuate sharply. The peak in H_1 at around 900 Hz is due to a bending mode of the rail shown in Figure 4(b), and the dip in H_2 at around 700 Hz is an anti-resonance of the block which occurs between the rigid mode at low frequency and the first flexible mode at 1.47 kHz shown in Figure 4(c). H_2 fluctuates more than H_1, but it only has a small effect on the estimate of dynamic stiffness as a_b is much smaller than a_u at high frequencies. The peak in $A_b m_b$ at around 15 Hz is due to the resonance of the block-support system, as seen in Figure 3.

To evaluate the sensitivity of the results to the accelerometer positions used on the lower block, two additional layouts of the accelerometers were simulated in the finite element model, as shown in Figure 6(b). Loc0 represents the original accelerometer layout used in the experiments. It can be seen that the results for $A_b m_b$ corresponding to original accelerometer layout are close to 1 for a wider frequency range than the other two layouts, which justifies the choice of accelerometer positions A3/A4. These positions Loc0 were chosen in the experiment to be as close as possible to the nodal positions of both the first vertical bending mode of the block and the twisting mode.

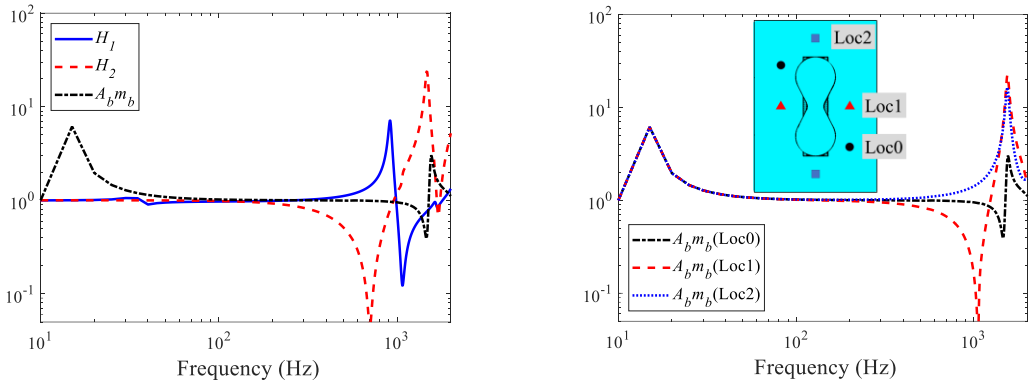

(a) (b)

Figure 6. Modification factor magnitudes and the transfer accelerance magnitude A_b (normalised by the block mass m_b): (a) H_1, H_2 and $A_b m_b$; (b) $A_b m_b$ corresponding to three different accelerometer layouts (shown in plan view)

4 Measured dynamic properties of the fastener

4.1 Rail pad

The dynamic stiffness (magnitude) of the rail pad derived from the measurements using the simplified formula (Eq. (3)) and the modified formula (Eq. (9), i.e. including the corrections obtained from the FE model) is shown in Figure 7 (a). For frequencies below 50 Hz, the modified curve fluctuates less sharply than the unmodified one, although some fluctuations remain. The two curves agree well with each other in the middle of the frequency range. However, between 400 Hz and 900 Hz, the unmodified curve tends to rise with increasing frequency, whereas the modified curve is relatively flat. It can be noticed that the stiffness curve obtained from the modified formula is flatter over a wider frequency range (50 Hz-900 Hz) than the unmodified one (50 Hz-400 Hz), as also found in the simulations (Figure 5(a)). With regard to the phase of the rail pad stiffness (Figure 7 (b)), the effect of the modification is less significant. The phase is relatively flat in the range 80–700 Hz but has large fluctuations outside this range.

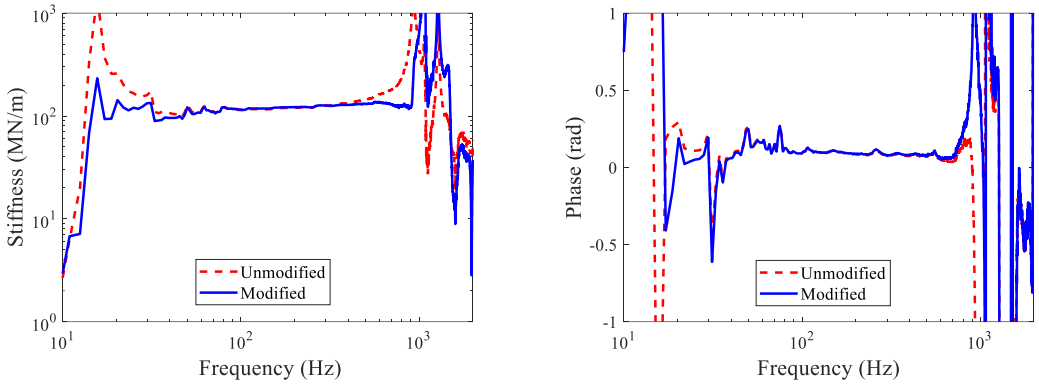

(a) (b)

Figure 7. Dynamic stiffness obtained from modified and simplified formulae under preload of 30 kN: (a) magnitude-frequency curves; (b) phase-frequency curves

To investigate the cause of the fluctuations of the stiffness curves below 50 Hz and above 900 Hz, the accelerations at A3 and A4 caused by the dynamic excitation are compared with the background vibration in Figure 8. It is clear that the accelerations at A3 and A4 in the dynamic test are not contaminated by background noise except for frequencies below 10 Hz. Therefore, the remaining fluctuations appear to result from the properties of the test rig, or differences between the correction factors derived from the finite element model and those that apply in reality.

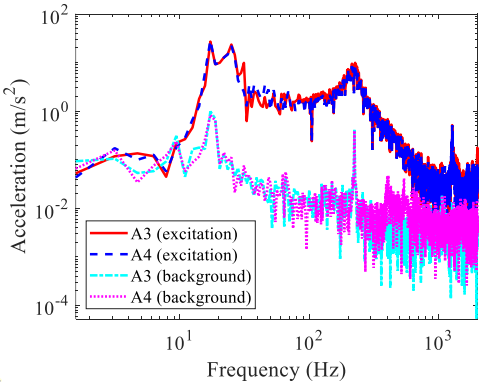

Figure 8. Accelerations at A3 and A4 caused by dynamic excitation and background vibration

Figure 9(a) shows the stiffness magnitude curves obtained from the modified formula for different preloads. The stiffness value of the rail pad gradually increases with the increase of the preload. On the double logarithmic scale, the stiffness shows a linear increasing trend with frequency within the frequency range 50–900 Hz.

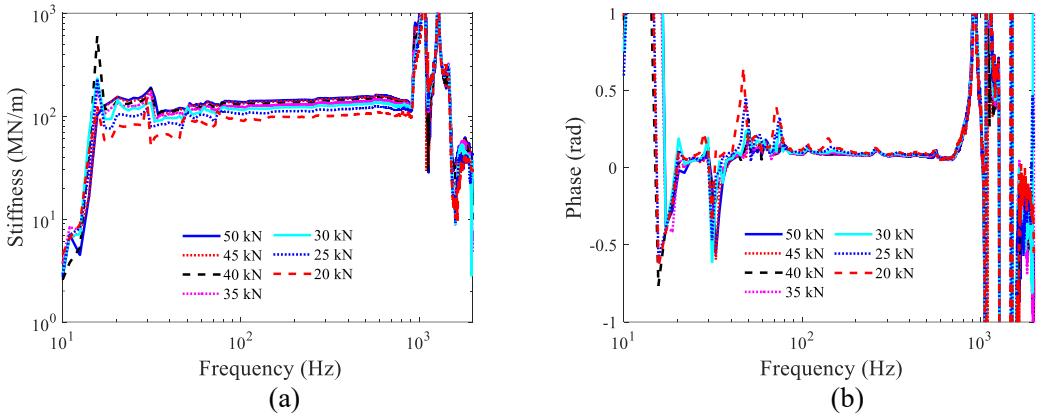

Figure 9. Stiffness magnitude and phase of the rail pad under various preloads: (a) stiffness magnitude; (b) phase

The corresponding phase under different preloads is shown in Figure 9(b). For frequencies below 80 Hz and above 700 Hz, the phase curves again show irregular fluctuations and are therefore considered unreliable. Within the frequency range 80–700 Hz, the phase value is within the range 0.1–0.15 rad, and the phase is approximately linearly related to log frequency. Considering the fact that the loss factor η is approximately equal to the phase angle ϕ ($\eta = \tan\phi \approx \phi$) when the phase angle is small, the loss factor also shows a linear dependence on log frequency within this frequency range.

The relationship between the stiffness magnitude and frequency within the frequency range 50–900 Hz, as well as the relationship between the loss factor and frequency within the frequency range 80–700 Hz, were fitted with linear functions in the (double) logarithmic scale. This allows the stiffness and loss factor to be extrapolated to frequencies beyond these frequency ranges. For rail transit bridges, frequencies such as 60 Hz, 200 Hz and 600 Hz are often prominent in the noise spectrum [44, 45]. Therefore, the stiffness as well as the damping loss factor at these frequencies have been extracted from the fitted functions and plotted against preload in Figure 10. The stiffness magnitude increases with the increase of preload, whereas the damping loss factor is largely independent of preload. The damping loss factor of the pad reduces slightly with increasing frequency.

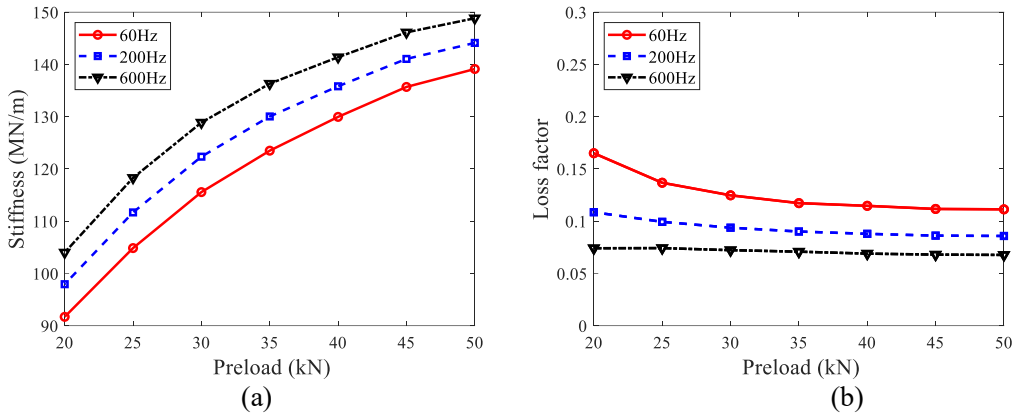

Figure 10. Fitted stiffness and damping loss factor of the rail pad under various preloads and frequencies: (a) stiffness; (b) damping loss factor

The damping loss factors of viscoelastic materials, such as rubbers, generally increase with frequency up to a peak in the transition zone and then fall with further increasing frequency [46]. The peak of the loss factor corresponds to the region of frequency at which the magnitude of the dynamic stiffness varies most strongly. Similar behaviour is found with respect to temperature; reducing temperature and increasing frequency are known to be equivalent. However, whereas these changes occur over a rather limited range of temperature (typically around 100°C) the same changes occur over typically 6-9 decades of frequency. The variation over one decade of frequency, such as shown here, is therefore likely to be small and could have either an increasing or decreasing trend.

Thompson et al. [20] and Fenander [21] showed results for a natural rubber railpad which contained a slight increase of damping loss factor with increasing frequency. Maes et al. [18] presented results on three rail pad materials that indicated a more strongly increasing loss factor with increasing frequency. Diehl et al. [47] showed loss factor results for a railpad which were largely independent of frequency. To summarise, the damping loss factors here are found to be largely independent of frequency, in some cases with a slight reduction with increasing frequency. The literature contains results that increase with frequency or are constant. In principle it is also possible for the loss factor to reduce with increasing frequency as found here.

4.2 Baseplate pad

The baseplate pad was measured together with the steel baseplate as it is wider than the rail foot used to excite the rail pad. Based on these measurements of the baseplate pad, its dynamic properties have been determined using the modified formula, as shown in Figure 11. The linear relationships with frequency in the double logarithmic scale are fitted within the frequency range 50–600 Hz, because the frequencies above 600 Hz are affected by the internal resonance as shown by the simulations in Figure 5(b).

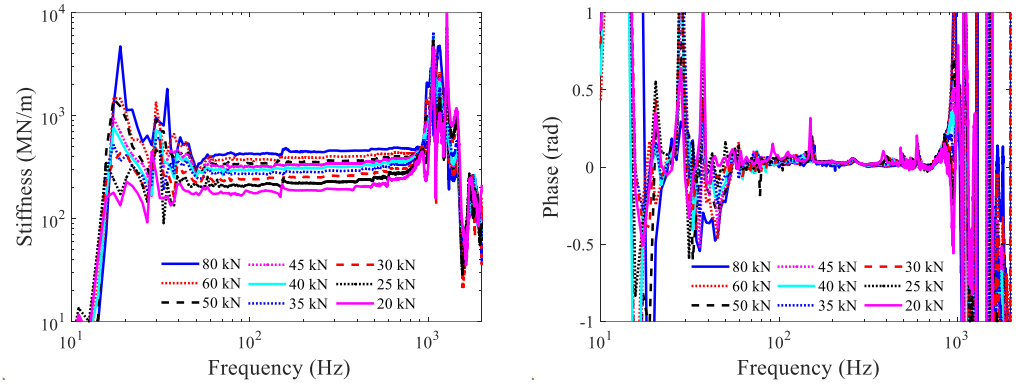

(a) (b)

Figure 11. Stiffness magnitude and phase of the baseplate pad under various preloads: (a) stiffness magnitude; (b) phase

Figure 12 shows the stiffness magnitude and loss factor of the baseplate pad under the corresponding frequencies and preloads. Compared with the rail pad, the baseplate pad has a higher stiffness and a lower damping loss factor for the same frequency and preload. The stiffness is more strongly dependent on both the preload and the frequency, which seems to contradict the fact that the loss factor of the baseplate pad is smaller. However, it seems from Figure 5(b) that the results at 600 Hz are already affected by proximity to the internal resonance at around 1 kHz and this will affect the curve fitting to some extent.

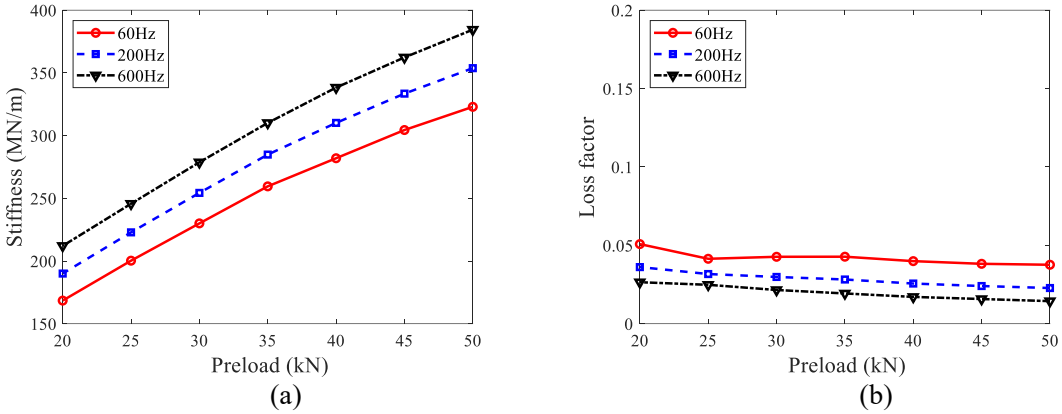

Figure 12. Fitted stiffness and damping loss factor of the baseplate pad under various preloads and frequencies: (a) stiffness; (b) damping loss factor

4.3 Whole fastener

The measured dynamic properties of the whole fastener were also obtained using the modified method and fitted by a linear function in the double logarithmic scale within the frequency range 50–400 Hz, avoiding the frequency range of the internal resonance seen in the simulations in Figure 5(c). Similar to the properties of the rail pad and baseplate pad, the stiffness value increases with the increase of preload as well as frequency. Figure 13 shows the fitted dynamic properties of the whole fastener under the specified frequencies and preloads. As expected, it can be found from Figures 10, 12, and 13 that, for a given frequency and preload, the stiffness of the whole fastener is lower than that of the individual components, while the loss factor of the whole fastener mostly lies between the loss factors of the two components.

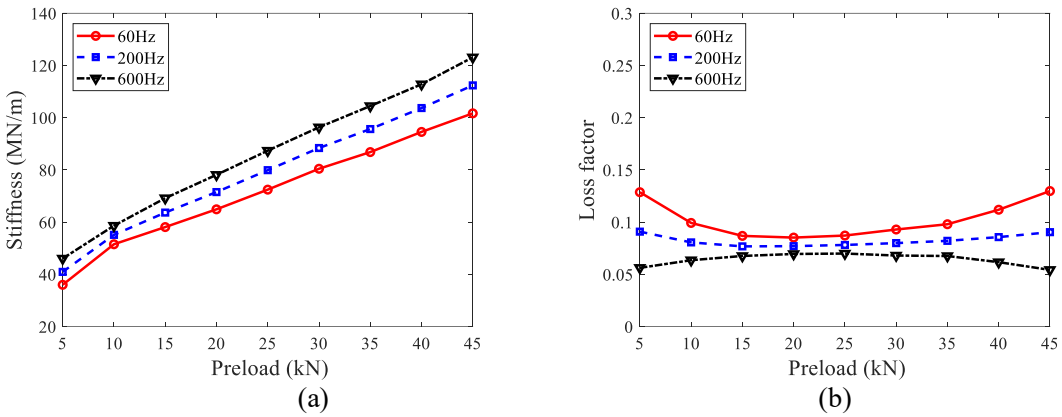

Figure 13. Fitted stiffness and damping loss factor of the whole fastener under various preloads and frequencies: (a) stiffness; (b) damping loss factor

5 Verification of test results

As the fastener components and the whole fastener system were tested separately, the test results can be verified by comparing the dynamic stiffness of the whole fastener with the combined dynamic stiffness of the components.

5.1 Based on measured dynamic stiffness

At low frequencies, the structure of the rail pad and baseplate pad can be regarded as two springs in series, although the simplification causes some errors at high frequencies due to the neglected mass. Based on this, the stiffness of the rail pad, baseplate pad and whole fastener should satisfy the relationship:

$$\frac{1}{K_w} = \frac{1}{K_u} + \frac{1}{K_l} \tag{10}$$

where K_w is the stiffness of the whole fastener system, K_u is the stiffness of the upper rail pad, K_l is the stiffness of the lower baseplate pad.

Based on the above formula, the dynamic stiffness of the whole fastener was derived by using the measured dynamic stiffnesses of the rail pad and baseplate pad. Then, the results were compared with the measured dynamic stiffness of the whole fastener. All the stiffness values involved in this section were obtained using the modified method based on Eq. (9). The results are given in Figure 14 for two values of preload and show good agreement. In the range 50–800 Hz, the maximum deviation is about 20%, which verifies the correctness of the experiment and the modification procedure. The deviation at the higher end of the frequency range results from the effect of the missing mass in the simplified spring-spring system.

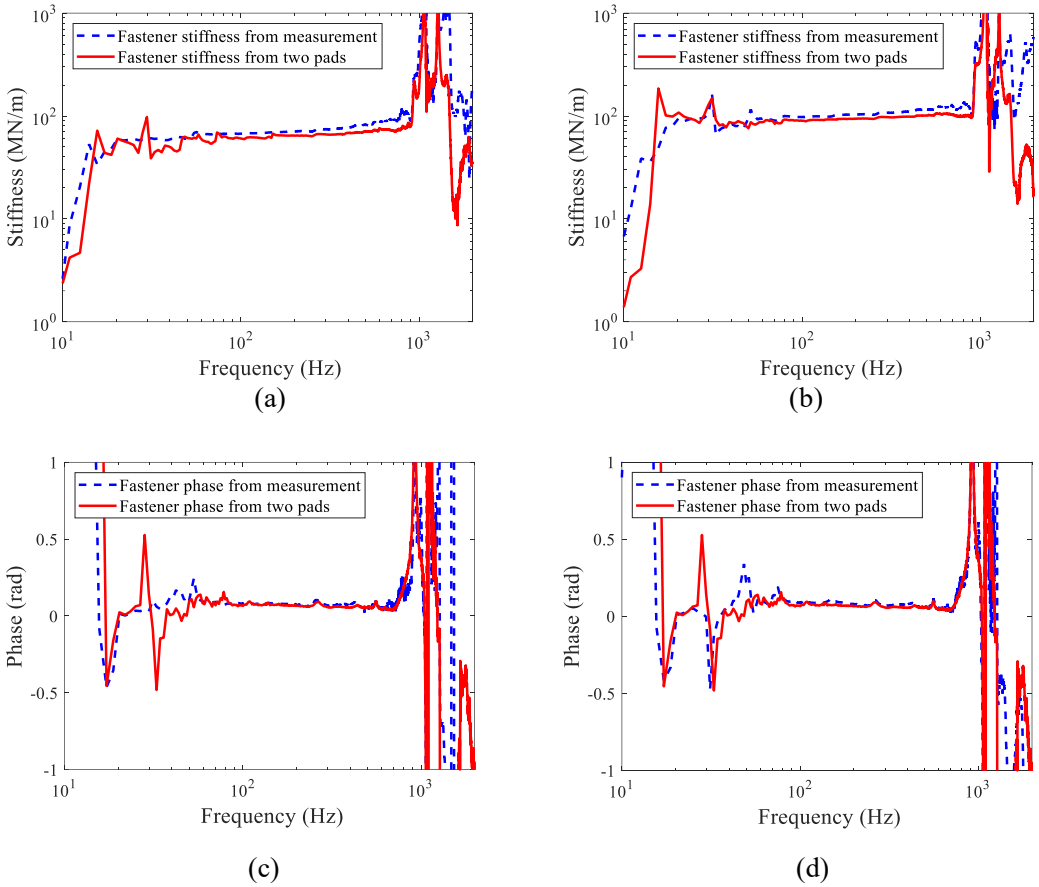

Figure 14. Comparison of the measured dynamic properties of the whole fastener and that calculated from the measured stiffness of the two pads in series: (a) stiffness magnitude at preload 20 kN; (b) stiffness magnitude at preload 40 kN; (c) phase at preload 20 kN; (d) phase at preload 40 kN

5.2 Based on fitted stiffness and intermediate mass

Due to the influence of the inertia characteristic of the steel plate in the high frequency region, the above relation cannot fully describe the dynamic characteristics of the baseplate. Therefore, the fastener system was represented as a spring-mass-spring system, and the combined dynamic stiffness obtained from the components (the springs and mass) was compared with the result for the whole system. For the components, the fitted stiffness functions were used. The stiffness of the whole fastener system can be expressed as:

$$K_w{}' = \frac{K_u{}' K_l{}'}{K_u{}' + K_l{}' - m_e\omega^2} \tag{11}$$

where $K_w{}'$ is the total dynamic stiffness of the whole fastener system; $K_u{}'$ is the fitted dynamic stiffness of the upper rail pad; $K_l{}'$ is the fitted dynamic stiffness of the lower baseplate pad; m_e means the effective mass of the intermediate steel plate. The effective mass m_e is

determined from the finite element model of the fastener by constraining the bottom of the lower rubber pad and applying a dynamic force distributed over the upper rail pad. The curve of m_e against frequency is shown in Figure 15. The effective mass of the steel plate remains roughly constant in the frequency range below 800 Hz, and fluctuates at around 1 kHz due to the internal resonance. The figure also shows that the effective mass is less than the actual mass over the entire frequency range. This is because the upper rail pad has a significantly smaller area than the intermediate steel plate. As a result, not all parts of the steel plate transfer load when the upper surface of the rail pad is loaded. This is illustrated in Figure 16 which shows the vertical displacement of the steel plate when a unit force is distributed over the surface of the rail pad, indicating that the steel plate undergoes quasi-static bending even at low frequencies.

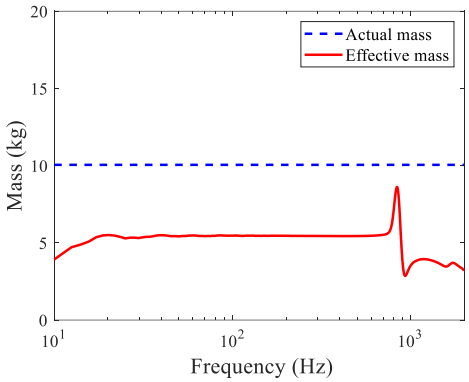

Figure 15. Actual mass and effective mass of the steel plate

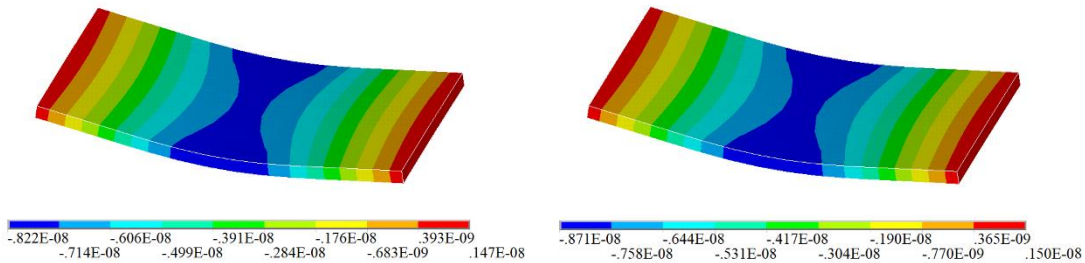

(a) (b)

Figure 16. Vertical displacement of the steel plate under unit force: (a) 20 Hz; (b) 200 Hz

The dynamic stiffness of the whole fastener obtained from the above formula is compared with the measured stiffness obtained using the revised method in Figure 17 (a) and (b) for the

same two values of preload. The two curves agree well in the range 20–900 Hz, which again indicates the effectiveness of the dynamic performance test and stiffness fitting. Above 900 Hz, the two curves have a certain deviation, which is mainly caused by the error of test rig. Figure 17 (c) and (d) show the corresponding phase curves which similarly show good agreement in the frequency range 50–700 Hz.

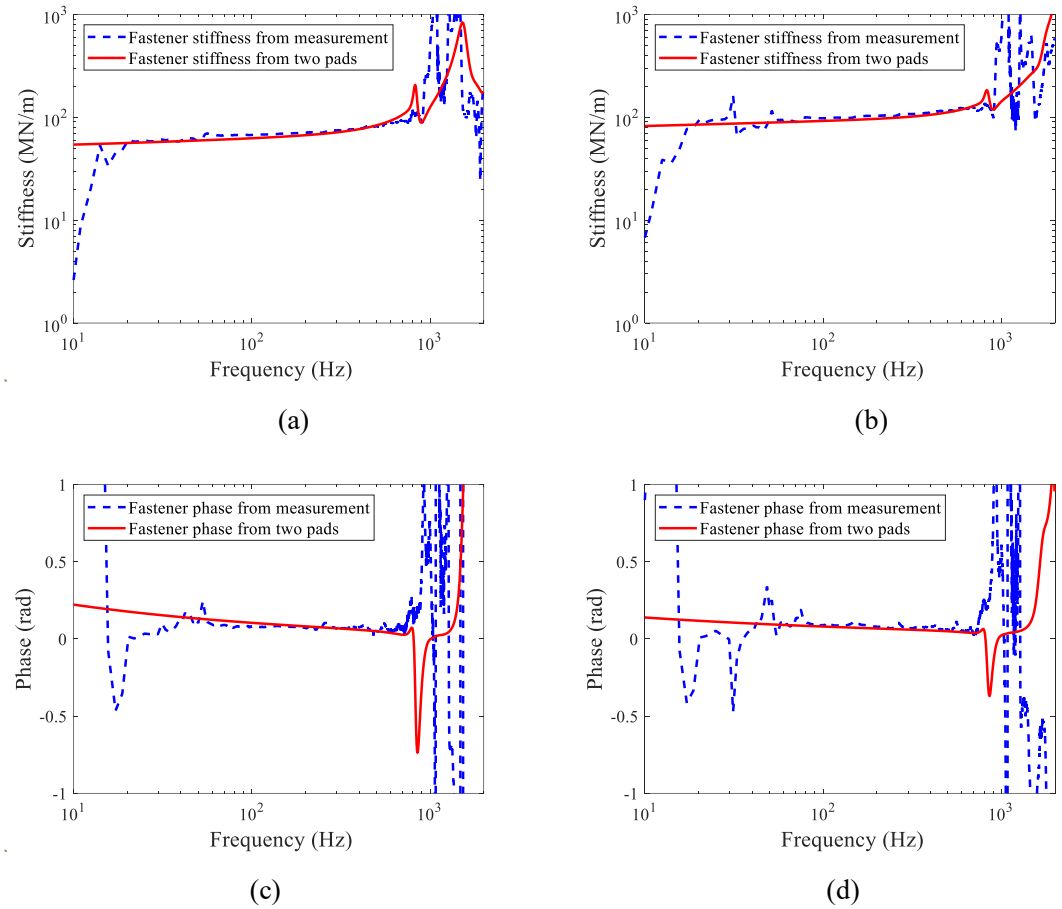

Figure 17. Comparison of the measured dynamic properties of the whole fastener and that calculated from fitted dynamic properties of the two pads and the steel plate in series: (a) stiffness magnitude at preload 20 kN; (b) stiffness magnitude at preload 40 kN; (c) phase at preload 20 kN; (d) phase at preload 40 kN

5.3 Based on field measured track decay rate

The track decay rate (TDR) is commonly used to describe the attenuation of rail vibration amplitude along the track [48, 49]. It is strongly influenced by the fastener stiffness, especially at the frequencies at which the TDR drops sharply. As a result, the field measured TDR can be utilized to verify the fastener stiffness measured in this study by using a numerical model of the

track. The TDR can be directly measured by hammer impact or indirectly estimated through measured rail vibration during the pass-by of trains [50]. The latter method has been applied to obtain the track decay rate of an elevated urban rail transit line adopting the WJ-2A fastener. Figure 18 compares the field measured TDR (from Ref [51] using the energy iteration method) with those calculated from the track-bridge system with different fastener models. Three spans of simply-supported girders each with length 30 m were considered although they mainly influence the TDR in the low frequency range. The rail is modelled as infinite Timoshenko beam model and it is then connected to the girders through discrete fasteners with a spacing of 0.6 m. The fasteners are represented by the two models as follows: the constant stiffness model of 40 MN/m (measured by the supplier using static method) and damping loss factor of 0.05; and the two-stage fastener model considering the effective mass for the baseplate and measured frequency-dependent complex stiffness of the rail pad and baseplate pad under the preload of 20 kN. The driving point and transfer mobilities of the rail are then calculated by applying a unit force on the rail at the middle span of the centre girder. These are used to determine the TDRs based on the standard method [48]. It can be seen from Figure 18 that the calculated TDRs with the frequency-dependent stiffness fastener model match the measured values better than the constant stiffness model especially around 200 Hz where the TDR drops sharply. Better agreement is also seen on average at high frequencies. This indicates the frequency-dependent stiffness measured in this study can be used to model the track with higher accuracy. It is noted that the measured TDR is subject to some measurement errors in the frequency range of interest, especially below 160 Hz where the TDR is high due to relatively large noise in the measured rail acceleration. The differences between the measured and calculated results above 1000 Hz are also affected by neglecting the sectional deformation of the rail [50].

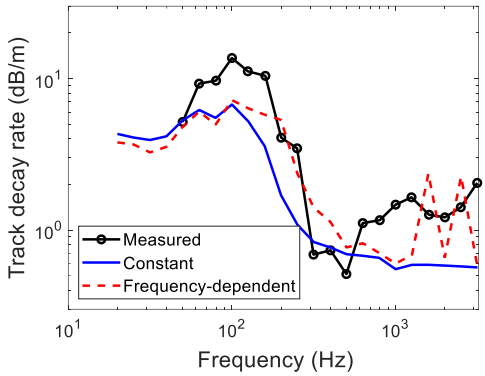

Figure 18. Comparison of field measured track decay rate with those calculated from various fastener models

6 Constitutive model of the fastener

The linear fitting on a double logarithmic scale conducted in the previous section of the dynamic stiffness obtained from the revised method can simulate the measured stiffness reliably within a certain frequency range, but the parameters obtained have no clear physical significance. In the following, curve fitting and parameter identification will be carried out based on the widely used fractional derivative Kelvin-Voigt (FDKV) model.

6.1 FDKV model

For viscoelastic materials, their constitutive equation can be represented by the FDKV model, which is written as [28, 52]:

$$\sigma(t) = \mu_1 \varepsilon(t) + \nu_1 D^{\gamma}[\varepsilon(t)] \tag{12}$$

where σ is the stress, ε is the strain, μ_1 is the elastic modulus, ν_1 is the viscosity coefficient, and D^{γ} means the fractional derivative operator, defined by

$$D^{\gamma}x(t) = \frac{1}{\Gamma(1-\gamma)}\frac{d}{dt}\int_0^t \frac{x(\tau)}{(t-\tau)^{\gamma}}d\tau \tag{13}$$

where Γ is the Gamma function ($\Gamma(z) = \int_0^{\infty} t^{z-1}e^{-t}dt$), and γ is the derivative order ($0 < \gamma < 1$).

By taking Fourier transforms, the complex modulus of the FDKV model can be expressed as:

$$Y^*(\omega) = \frac{\sigma(\omega)}{\varepsilon(\omega)} = Y_s + \mathrm{i}Y_l \tag{14}$$

where Y_s is the storage modulus ($Y_s = \mu_1 + \omega^{\gamma}\nu_1 \cos\frac{\gamma\pi}{2}$), and Y_l is the loss modulus ($Y_l =$

$\omega^{\gamma}\nu_1 \sin\frac{\gamma\pi}{2}$).

Based on the above expressions, the magnitude of Y^* and the damping loss factor η can be written as:

$$|Y^*| = \sqrt{{Y_s}^2 + {Y_l}^2} = \sqrt{{\mu_1}^2 + 2\mu_1\omega^{\gamma}\nu_1 \cos\frac{\gamma\pi}{2} + \omega^{2\gamma}{\nu_1}^2} \quad (15)$$

$$\eta = \frac{Y_l}{Y_s} = \frac{\omega^{\gamma}\nu_1 \sin\frac{\gamma\pi}{2}}{\mu_1 + \omega^{\gamma}\nu_1 \cos\frac{\gamma\pi}{2}} \quad (16)$$

These two expressions contain three parameters (μ_1, ν_1 and γ). In the next section, a genetic algorithm function built in MATLAB software is used for numerical fitting and parameter identification based on the measured dynamic stiffness results.

6.2 Model parameter fitting

The measured stiffness magnitude and loss factor data were converted to 1/3 octave frequency bands by averaging all values in each frequency band so that fewer data points are used to fit the parameters of the FDKV model. In the genetic algorithm, the difference between the fitted values (stiffness magnitude and loss factor) and the original data were divided by the original value to calculate the relative errors, and the sum of the squared relative errors was used as the objective function. Various weightings were tested for the stiffness relative error and loss factor relative error. Use of equal weightings was found to achieve a suitable trade-off in fitting these two dynamic properties.

6.2.1 Rail pad

Figure 19 shows the results of fitting the measured stiffness magnitude and loss factor of the upper rail pad using the FDKV model. The FDKV model can fit the data points well, for both stiffness magnitude and loss factor. This is because the rail pad is made of viscoelastic material, and the FDKV model gives a good characterization of viscoelastic material properties. The parameters fitted by the FDKV model for the rail pad under different preloads are listed in Table 4.

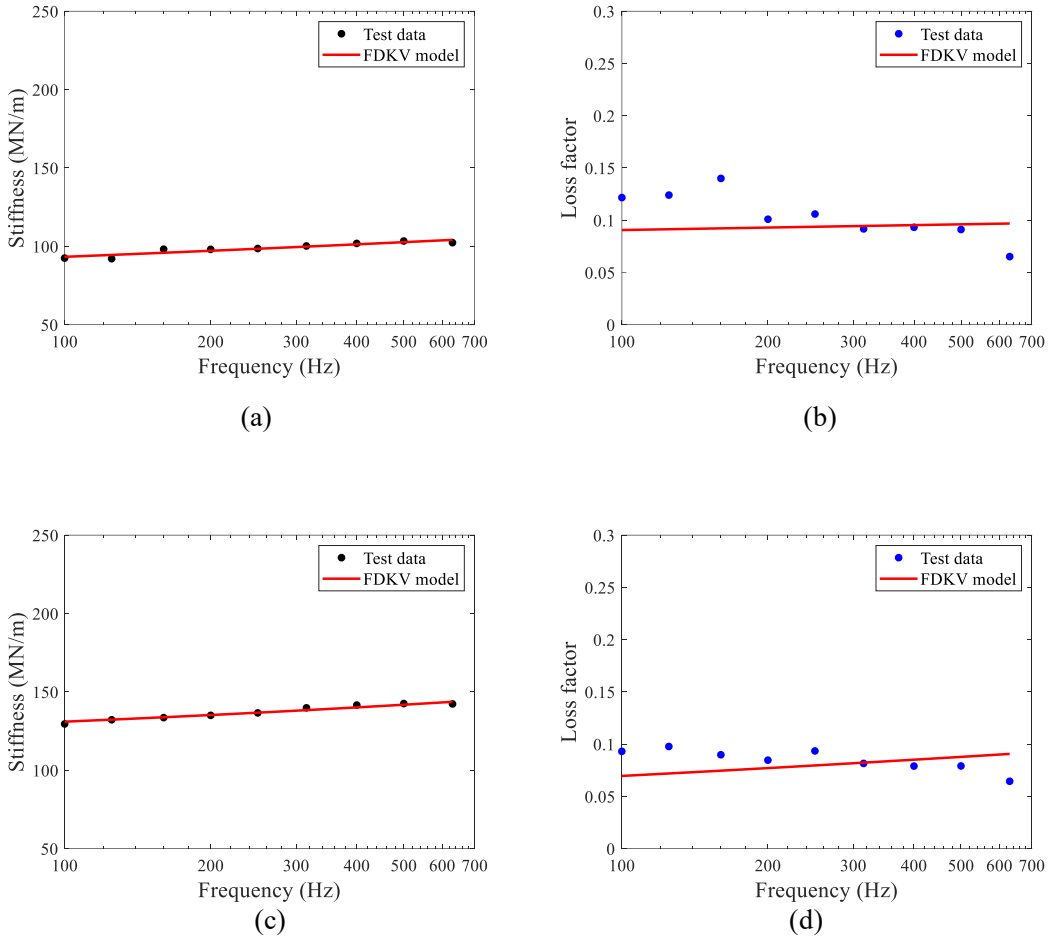

Figure 19. Dynamic properties of the rail pad from the test results in 1/3 octave bands and the fitted FDKV model: (a) stiffness magnitude at preload 20 kN; (b) damping loss factor at preload 20 kN; (c) stiffness magnitude at preload 40 kN; (d) damping loss factor at preload 40 kN

Table 4 Fitted parameters of the FDKV model for the rail pad

Preload (kN)	μ_1 (MN/m)	ν_1 (MN/m/(rad/s)$^\gamma$)	γ
20	50.9	19.56	0.12
25	66.7	16.82	0.14
30	72.1	19.79	0.13
35	86.4	14.72	0.15
40	83.2	20.79	0.13
45	90.8	18.59	0.14

6.2.2 Lower baseplate pad

The FDKV model of the lower rubber pad can be obtained by fitting the dynamic properties of the baseplate pad in low frequency range (below 600 Hz as discussed in Section 4.2), as shown in Figure 20. Under different preloads, the fitting parameters of the lower rubber pad were obtained as listed in Table 5.

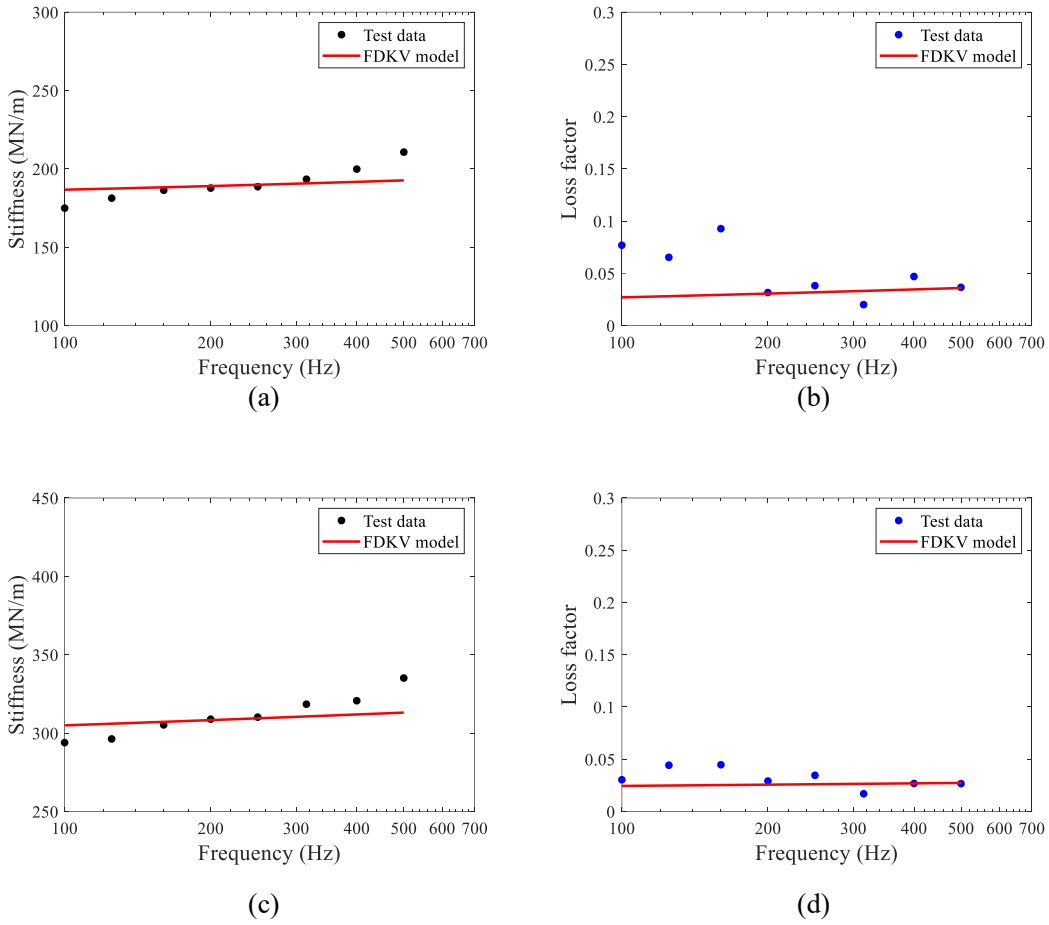

Figure 20. Dynamic properties of the lower rubber pad from the test results at 1/3 octave bands and the fitted FDKV model: (a) stiffness at preload 20 kN; (b) damping loss factor at preload 20 kN; (c) stiffness at preload 40 kN; (d) damping loss factor at preload 40 kN

Table 5 Fitted parameters of the FDKV model for the lower rubber pad

Preload (kN)	μ_1 (MN/m)	ν_1 (MN/m/(rad/s)$^\gamma$)	γ
20	176.4	2.17	0.26
25	207.4	2.47	0.26
30	234.7	3.89	0.23
35	262.2	4.98	0.21
40	288.9	4.63	0.22
45	309.7	5.90	0.20

6.2.3 Whole fastener

Unlike the rail pad, the whole fastener does not have the dynamic characteristics of a pure rubber material, as it also contains the steel plate. Therefore, the FDKV model of the whole fastener is represented by combining the FDKV models of the two rubber pads with the influence of the intermediate steel plate.

The influence of the intermediate steel plate was considered using a frequency-dependent effective mass m_e as described in Section 5.2. Similar to the Eq. (11), the stiffness of the whole fastener can be obtained through the FDKV models of the two pads together with the effective mass of the intermediate steel plate, as shown in Figure 21. It can be seen that the combined models fit well with the measured results in a wide frequency range. Similar to Figure 17, fluctuations appearing at around 1 kHz are caused by the internal resonance of the intermediate steel plate.

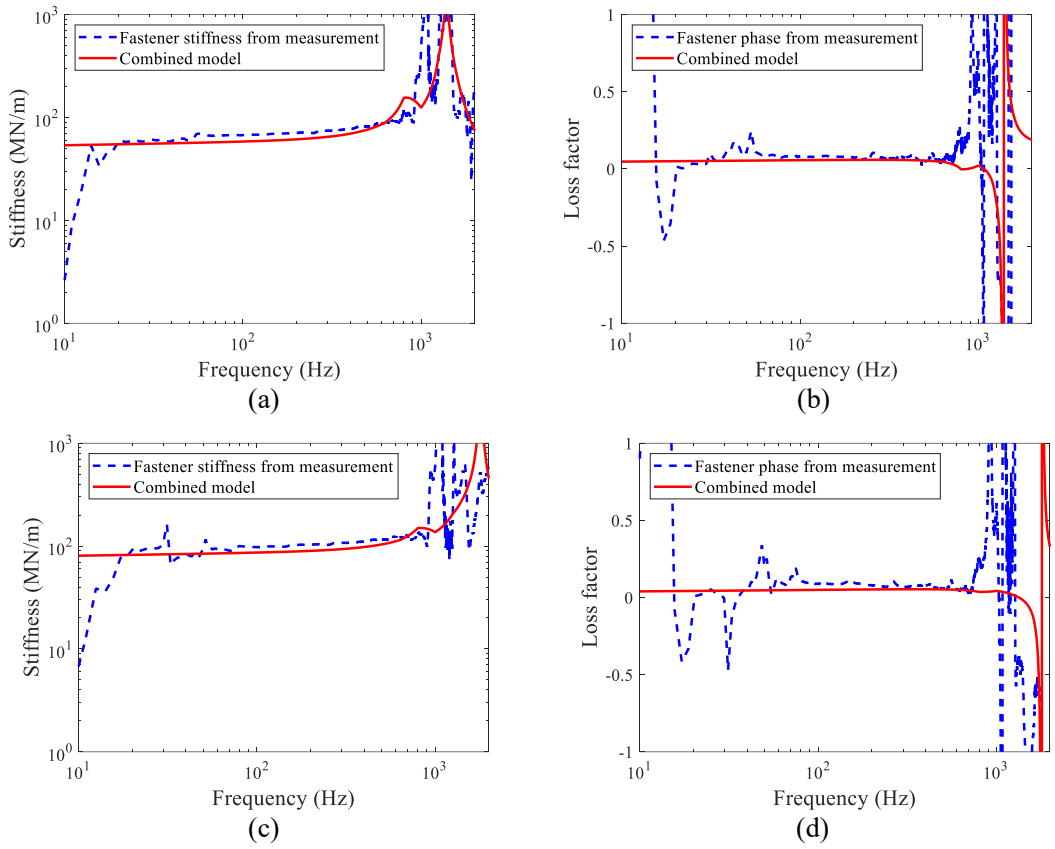

Figure 21. Dynamic properties of the whole fastener from the test results and the combined models: (a) stiffness at preload 20 kN; (b) damping loss factor at preload 20 kN; (c) stiffness at preload 40 kN; (d) damping loss factor at preload 40 kN

7 Conclusions

The load- and frequency-dependence of the dynamic stiffness behaviour of a WJ-2A two-stage rail fastener has been investigated using the indirect measurement method. The measurement results cover the frequency range 30 to 1000 Hz.

Using a numerical model of the test rig it has been shown that there are significant differences between the response at the measurement positions and at the ideal positions at the interfaces between the fastener and the rig. Consequently, this can be identified as the cause of measurement artefacts observed above 500 Hz. A correction procedure has been proposed based on the numerical results to reduce the effect of these artefacts and extend the usable frequency range. The influence of the test equipment on the measurement results should not be ignored and appropriate correction factors should be used to minimise measurement artefacts. Suitable correction factors have been obtained from the numerical model.

The stiffness magnitude of the rail pad, baseplate pad, and whole fastener system increases strongly with increasing static preload and increases weakly with increasing frequency. However, the damping loss factors are not strongly dependent on either preload or frequency and are found to reduce slightly with increasing frequency.

To account for the frequency-dependence of the materials, the fractional derivative Kelvin-Voigt (FDKV) model has been fitted to the measurement results for the two rubber pads. It can adequately describe the frequency-dependent properties of the rubber pads at different preloads. However, the dynamic stiffness of the whole fastener system is influenced by both pads as well as the steel baseplate. It can be estimated from a combination of the FDKV models of the two pads together with the equivalent mass of the baseplate. It is important to take account of this to include the internal resonance of the baseplate assembly appearing at around 1 kHz.

Acknowledgements

The study was supported by the National Natural Science Foundation of China (No. 51878501 and 51678576), and National Engineering Laboratory for High-speed Railway Construction Technology (Open Fund Project HSR201902). The measurements were performed with the help of Boniface Hima of University of Southampton, and the data analysis was partly conducted by Manfei Shi of Tongji University. Their work is gratefully

acknowledged.

References

[1] N. Gil-Negrete, J. Vinolas, L. Kari, A simplified methodology to predict the dynamic stiffness of carbon-black filled rubber isolators using a finite element code, Journal of Sound and Vibration 296(4-5) (2006) 757-776.
[2] D.J. Thompson, J.W. Verheij, The dynamic behaviour of rail fasteners at high frequencies, Applied Acoustics 52(1) (1997) 1-17.
[3] M. Sol-Sanchez, F. Moreno-Navarro, M. Carmen Rubio-Gamez, The use of elastic elements in railway tracks: A state of the art review, Construction and Building Materials 75 (2015) 293-305.
[4] K.L. Knothe, S. Grassie, Modelling of Railway Track and Vehicle/Track Interaction at High Frequencies, Vehicle System Dynamics 22 (1993) 209-262.
[5] I.A. Carrascal, A. Perez, J.A. Casado, S. Diego, J.A. Polanco, D. Ferreno, J.J. Martin, Experimental study of metal cushion pads for high speed railways, Construction and Building Materials 182 (2018) 273-283.
[6] N. Vincent, P. Bouvet, D.J. Thompson, P.E. Gautier, Theoretical optimization of track components to reduce rolling noise, Journal of Sound and Vibration 193(1) (1996) 161-171.
[7] M. Oregui, Z. Li, R. Dollevoet, An investigation into the vertical dynamics of tracks with monoblock sleepers with a 3D finite-element model, Proceedings of the Institution of Mechanical Engineers, Part F: Journal of Rail and Rapid Transit 230(3) (2016) 891-908.
[8] S. Zhu, C. Cai, P.D. Spanos, A nonlinear and fractional derivative viscoelastic model for rail pads in the dynamic analysis of coupled vehicle–slab track systems, Journal of Sound and Vibration 335 (2015) 304-320.
[9] K. Wei, Y. Dou, F. Wang, P. Niu, P. Wang, Z. Luo, High-frequency random vibration analysis of a high-speed vehicle–track system with the frequency-dependent dynamic properties of rail pads using a hybrid SEM–SM method, Vehicle System Dynamics 56 (2018) 1838-1863.
[10] K. Wei, F. Wang, P. Wang, Z.X. Liu, P. Zhang, Effect of temperature- and frequency-dependent dynamic properties of rail pads on high-speed vehicle–track coupled vibrations, Vehicle System Dynamics 55(3) (2017) 351-370.
[11] G. Squicciarini, D.J. Thompson, M.G. Toward, R.A. Cottrell, The effect of temperature on railway rolling noise, Proceedings of the Institution of Mechanical Engineers, Part F: Journal of Rail and Rapid Transit 230 (2015) 1777-1789.
[12] D.J. Thompson, C.J.C. Jones, T.X. Wu, A. de France, The influence of the non-linear stiffness behaviour of rail pads on the track component of rolling noise, Proceedings of the Institution of Mechanical Engineers, Part F: Journal of Rail and Rapid Transit 213(4) (1999) 233-241.
[13] F. Yang, P. Wang, K. Wei, F. Wang, Investigation on nonlinear and fractional derivative Zener model of coupled vehicle-track system, Vehicle System Dynamics 58 (2019) 864-889.
[14] ISO(10846-1), Acoustics And Vibration - Laboratory Measurement of Vibro-acoustic Transfer Properties of Resilient Elements - Part 1: Principles and Guidelines, (1997).
[15] ISO(10846-2), Acoustics And Vibration - Laboratory Measurement of Vibro-acoustic Transfer Properties of Resilient Elements - Part 2: Dynamic Stiffness of Elastic Supports for Translatory Motion - Direct Method, (1997).
[16] ISO(10846-3), Acoustics And Vibration - Laboratory Measurement Of Vibro-acoustic Transfer Properties Of Resilient Elements - Part 3: Dynamic Stiffness Of Elastic Supports For Translatory Motion - Indirect Method, (1997).
[17] S. Kaewunruen, A.M. Remennikov, An Alternative Rail Pad Tester for Measuring Dynamic Properties of Rail Pads Under Large Preloads, Experimental Mechanics 48(1) (2008) 55-64.
[18] J. Maes, H. Sol, P. Guillaume, Measurements of the dynamic railpad properties, Journal of Sound and Vibration 293(3-5) (2006) 557-565.
[19] J. Park, S. Ahn, J. Kim, H.-I. Koh, J. Park, Direct determination of dynamic properties of railway tracks for flexural vibrations, European Journal of Mechanics-A/Solids 61 (2017) 14-21.
[20] D.J. Thompson, W.J.V. Vliet, J.W. Verheij, Developments of the indirect method for measuring the high frequency dynamic stiffness of resilient elements, Journal of Sound and Vibration 213(1) (1998) 169-188.
[21] Å. Fenander, Frequency dependent stiffness and damping of railpads, Proceedings of the Institution of Mechanical Engineers -- Part F 211(1) (1997) 51-62.
[22] J. van't Zand, Assessment of dynamic characteristics of rail pads, Rail Engineering International 23(4) (1994) 15-17.
[23] A.P. de Man, Dynatrack: A survey of dynamic railway track properties and their quality, Technische Universiteit Delft, 2002.
[24] A.M. Remennikov, S. Kaewunruen, Determination of dynamic properties of rail pads using an instrumented hammer impact technique, Acoustics Australia 33 (2005) 63-67.

[25] S. Kaewunruen, A.M. Remennikov, Field trials for dynamic characteristics of railway track and its components using impact excitation technique, NDT & E International 40(7) (2007) 510-519.
[26] S. Kaewunruen, A.M. Remennikov, State Dependent Properties of Rail Pads, Engineers Australia2009.
[27] K. Wei, Z.X. Liu, Y.C. Liang, P. Wang, An investigation into the effect of temperature-dependent stiffness of rail pads on vehicle-track coupled vibrations, Proceedings of the Institution of Mechanical Engineers Part F Journal of Rail & Rapid Transit 0 (2017) 1-11.
[28] K. Wei, Q. Yang, Y. Dou, F. Wang, P. Wang, Experimental investigation into temperature- and frequency-dependent dynamic properties of high-speed rail pads, Construction and Building Materials 151 (2017) 848-858.
[29] M.L. Williams, R.F. Landel, J.D. Ferry, The Temperature Dependence of Relaxation Mechanisms in Amorphous Polymers and Other Glass-forming Liquids, Journal of the American Chemical Society 77(14) (1955) 3701-3707.
[30] L. Liu, Z. Zuo, Y. Zhou, J. Qin, Insights into the Effect of WJ-7 Fastener Rubber Pad to Vehicle-Rail-Viaduct Coupled Dynamics, Applied Sciences 10(5) (2020).
[31] L.B. Eldred, W.P. Baker, A.N. Palazotto, Kelvin-Voigt versus fractional derivative model as constitutive relations for viscoelastic materials, Aiaa Journal 33 (1995) 547-550.
[32] N. Gil-Negrete, J. Vinolas, L. Kari, A Nonlinear Rubber Material Model Combining Fractional Order Viscoelasticity and Amplitude Dependent Effects, Journal of Applied Mechanics 76(1) (2009).
[33] Y. Honda, T. Saito, K. Wakabayashi, T. Kodama, S. Iwamoto, A Simulation Method for Crankshaft Torsional Vibration by Considering Dynamic Characteristics of Rubber Dampers, SAE Technical Paper, 1989.
[34] M. Sasso, G. Palmieri, D. Amodio, Application of fractional derivative models in linear viscoelastic problems, Mechanics of Time Dependent Materials 15(4) (2011) 367-387.
[35] D. Lei, Y. Liang, R. Xiao, A fractional model with parallel fractional Maxwell elements for amorphous thermoplastics, Physica A Statistical Mechanics & Its Applications 490 (2018) 465-475.
[36] F. Mainardi, Fractional calculus and waves in linear viscoelasticity : an introduction to mathematical models, Imperial College Press2010.
[37] M. Caputo, Linear Models of Dissipation whose Q is almost Frequency Independent—II, Geophysical Journal International 13 (1967) 529-539.
[38] H. Shi, P. Wu, A nonlinear rubber spring model containing fractional derivatives for use in railroad vehicle dynamic analysis, Proceedings of the Institution of Mechanical Engineers, Part F: Journal of Rail and Rapid Transit 230 (2016) 1745-1759.
[39] Q. Yang, H.B. Chen, Y.Y. Wang, Statistical Energy Analysis of Fractional Derivative Model-Based Rubber Vibration Isolating System, Applied Mechanics and Materials 437 (2013) 114-119.
[40] Arikoglu, Aytac, A new fractional derivative model for linearly viscoelastic materials and parameter identification via genetic algorithms, Rheologica Acta 53(3) (2014) 219-233.
[41] J.W. Verheij, Measuring sound transfer through resilient mountings for separate excitation with orthogonal translations and rotations, INTER-NOISE and NOISE-CON Congress and Conference Proceedings, 1980, pp. 723-726.
[42] J.W. Verheij, Multi-path sound transfer from resiliently mounted shipboard machinery : experimental methods for analyzing and improving noise control, Delft, The Netherlands, 1982.
[43] D.J. Tweten, Z. Ballard, B.P. Mann, Minimizing error in the logarithmic decrement method through uncertainty propagation, Journal of Sound and Vibration 333(13) (2014) 2804-2811.
[44] Q. Li, W.Q. Li, D.J. Wu, X.D. Song, A combined power flow and infinite element approach to the simulation of medium-frequency noise radiated from bridges and rails, Journal of Sound and Vibration 365 (2016) 134-156.
[45] X. Zhang, X. Li, J. Zhang, L. Song, Y. Li, A hybrid model for the prediction of low-frequency noise emanating from a concrete box-girder railway bridge, Proceedings of the Institution of Mechanical Engineers, Part F: Journal of Rail and Rapid Transit 230 (2015).
[46] A.D. Nashif, D.I.G. Jones, J.P. Henderson, Vibration damping, John Wiley & Sons, New York, 1985.
[47] R. Diehl, U. Kurze, P. Hofmann, Laboratory testing of elastic layers for railway application, 11th International Congress on Sound and Vibration, St Petersburg, Russia, 2004.
[48] E. 15461:2008+A1:2010, Railway applications – Noise emission – Characterization of the dynamic properties of track selections for pass by noise measurements, European Committee for Standardization, Brussels, 2010.
[49] D.J. Thompson, Railway noise and vibration: mechanisms, modelling and means of control, Elsevier, 2009.
[50] Q. Li, D. Thompson, M. Toward, Estimation of track parameters and wheel–rail combined roughness from rail vibration, Proceedings of the Institution of Mechanical Engineers, Part F: Journal of Rail and Rapid Transit 232 (2018) 1149-1167.
[51] Q. Li, D. Thompson, Prediction of rail and bridge noise from concrete railway viaducts using a multi-layer rail fastener model and a wavenumber domain method, Proceedings of the Institution of Mechanical Engineers, Part F: Journal of Rail and Rapid Transit 232 (2018) 1326-1346.
[52] F. Mainardi, G. Spada, Creep, Relaxation and Viscosity Properties for Basic Fractional Models in Rheology,

The European Physical Journal Special Topics 193 (2011) 133-160.